Integrated Potential Formulation of Unsteady Supersonic Aerodynamics for Interacting Wings

Kari Appa*
Bell Aerospace Textron, Buffalo, N. Y.
and
W. P. Jones†
Texas A and M University, College Station, Texas

A numerical integrated velocity potential method for the determination of unsteady aerodynamic forces on arbitrary interacting wings and tails in supersonic flow has been developed. Normal-wash and sidewash integrals have been derived. The longitudinal-wash integral remains to be derived. Singular integrals in the expressions for the velocity components have been evaluated in closed form. Lifting surfaces are represented by triangular elements defined by arbitrarily spaced characteristic lines and the true surface edges. The wake field is represented by rectangular strip elements. Small perturbation velocity potential distributions and generalized aerodynamic coefficients have been compared.

Nomenclature

a_0 = velocity of sound
k,k' = reduced frequencies, $\omega\ell/U, kM/\beta$
l = reference length
$\hat{l},\hat{m},\hat{n}$ = direction cosines of a normal
m = slope of a line
M = Mach number
n,v = unit normal, conormal
p = pressure
$\bar{Q}_{ij} = Q_{ij}/\rho U^2 \ell^3$ = generalized aerodynamic coefficients
S = surface of integration
r^2 = $(x_0-x)^2 - Z_0^2$
$R = [r^2 - (y_0-y)^2]^{1/2}$ = hyperbolic radius
t' = dimensional time
t = nondimensional time
T = transformation matrix for triangular elements
U = airstream velocity
u,v,w = induced velocity components; also termed as backwash, sidewash, and normal-wash components
W = influence coefficient matrix relating normal velocity and velocity doublets, Eq. (26)
x',y',z' = dimensional space coordinates
x,y,z = nondimensional space coordinates
$X \equiv (x,y,z)$ = field point at x,y,z
α = constant of a line
β = $[M^2-1]^{1/2}$
η = displacement normal to the lifting surface
η = y_0-y
ξ = x_0-x
ρ = air density
φ = velocity potential, a scalar quantity
φ' = $\varphi e^{ik'Mx}$
$\Delta\phi$ = vector of potential doublets
ψ_1,ψ_2,ψ = particular solutions of hyperbolic equation in supersonic conical flow
ω = circular frequency of harmonic motion, rad/sec
Ω = interpolation matrix function

Received May 16, 1975; presented as Paper 75-762 at the AIAA/ASME/SAE 16th Structures, Structural Dynamics, and Materials Conference, Denver, Colo., May 27-29, 1975; revision received Nov. 17, 1975. This work was performed for NASA under Contract NASI-12709. Robert W. Hess, at Langley Research Center, acted as Technical Monitor.

Index categories: Supersonic and Hypersonic Flow; Aeroelasticity and Hydroelasticity.

*Chief, Dynamic Analysis. Member AIAA.

†Distinguished Professor, Aerospace Engineering Department. Fellow AIAA.

Introduction

EFFICIENT and accurate prediction of unsteady aerodynamic forces on airplane configuration has been studied for over three decades. Source, doublet, and pressure superposition methods are the three major approaches that have received attention. The source superposition method gives a very simple, direct integral relationship between the potential and the downwash field (which is determined by the mode shapes) in the noninteracting case.[1] However, in the interacting case, the potential first is related to the source strength, and the source strengths in turn is related to the downwash distribution.[2] Thus, two sets of equations are required to solve the problem by this method. In addition, integration over wake regions and nonunique "diaphragms" is necessary as a part of the solution.

In the velocity potential method, there is a direct relationship between the downwash (the mode shapes) and the velocity potential.[3] Diaphragm regions are no longer necessary, and wake regions do not need detailed modeling, since their behavior is determined by trailing edge potentials of the wake-producing surface. The integral relations, which are more complicated than in the source superposition method, have been simplified considerably in the current work.

The pressure potential, or kernel function method, is a "direct" approach via a relation between downwash and pressures and aerodynamic coefficients.[4-6] This integral relations is, however, even more complicated than in the velocity potential approach. In the unsteady case, numerical methods have not been developed fully to permit the selection of simple pressure functions in each element, independent of other elements.

In each approach, analytical solutions for lift and moment distributions are available for a limited number of simple planforms. However, for arbitrary configurations, numerical methods are necessary. These may be classified broadly as

collocation and finite element methods. Collocation methods assume, a priori, certain mode shapes or series expansions of the unknown parameters such as pressures and doublet distributions. The coefficients of these series or modes are determined from a set of algebraic equations established by satisfying the integral relation only at an appropriate number of collocation points. The number of equations is comparatively low, and an efficient computation generally results for simple configurations.[7-9]

In finite element approaches, the integration over the dependence domain is replaced by the sum of integrations over a number of simple elemental domains (finite elements). Over each element area, the unknown parameter is expressed as a sum of simple functions. There exist a number of finite element variations, such as square, Mach and characteristics boxes, and triangular or quadrilateral elements. Numerical approaches differ also in the choice of functional variation within each element and in the integration methods over the elements.[10-18]

In Mach or characteristic box schemes, planform edges usually have been approximated by jagged representations, which result in fluctuating pressure over the whole surface. More recent versions of Mach box programs are described.[10-11] A triangular representation of the dependence domain using a linear distribution of sources was developed.[13-14] This method seemed to offer acceptable accuracies with far fewer elements than other methods. Using characteristic elements, a doublet superposition method based on Jones' integrated potential formulation was developed[16] for planar configurations. The kernel sine and cosine functions were expressed as parabolic interpolation functions within each element. Woodcock and York[17] extended this approach to interacting wings.

In this study, a method of handling the strong singular functions in the integral equations without the use of Hadamard's finite part technique has been developed. Closed-form integrals have been obtained for singular functions, whereas numerical integrations are employed for algebraically complicated but analytic functions. Normalwash and sidewash integrals have been derived. Area integrals have been transformed to contour integrals. A linear potential element model is discussed in the current work, including examples. The perburbation velocity potential distributions and generalized aerodynamic coefficients have been obtained and compared with available results from other sources.

Analytical Formulation

Basic Equations

In the formulation of the basic differential equations of potential flow, the velocity potential φ generally is chosen as a single scalar independent function, thereby reducing the number of dependent variables (from the velocity components u,v,w) by two. The velocity potential is related to the pressure through the unsteady Bernoulli's equation.

Using the following dimensionless form of the coordinates,

$$x=x'/\beta l, y=y'/l, z=z'/l, t=Ut'/l \tag{1}$$

the supersonic wave equation can be written as

$$-\frac{\partial^2\varphi'}{\partial x^2}+\frac{\partial^2\varphi'}{\partial y^2}+\frac{\partial^2\varphi'}{\partial z}+k'^2\varphi'=0 \tag{2}$$

where

$$\varphi'=\varphi e^{ik'Mx}$$

is the modified velocity potential, and $k'=kM/\beta$, in which $k=\omega l/U$ is the reduced frequency.

The solution to Eq. (2) has been obtained by Jones[3] by the use of the generalized Green's theorem and is given by the following integral relation

$$2\pi\varphi'(X_0)=\int\int_S\left[\varphi'(X)\frac{\partial\psi}{\partial v}-n\frac{\partial\varphi'}{\partial v}\right]dS \tag{4}$$

where ψ is a generalized Green's function related to two particular solutions satisfying Eq. (2), and $\partial(\ )/\partial v$ is a differential operator in the direction of the conormal to the surface at X.

The area of integration S extends over the domain of dependence, i.e., lifting surfaces and an artificial barrier ("diaphragm" and wake), which extends to separate the flow from the upper and lower surfaces of the lifting surfaces (Fig. 1). In numerical integration methods, the area of integration is represented by a number of flat finite elements. Integration over each panel can be performed in a transformed coordinate system such that the element lies parallel to the x-y plane in the transformed coordinates. Then the conormal derivative is simplified by the relation $\partial\varphi/\partial v=\partial\varphi/\partial z$. For thin lifting surfaces, the integration area can be reduced by noting that the discontinuous distributions of φ' and $\partial\varphi'/\partial z$ across the surfaces are such that

$$\Delta\varphi'=\varphi'_U-\varphi'_L \quad \begin{matrix}\text{(a velocity potential}\\ \text{doublet distribution)}\end{matrix} \tag{5}$$

and

$$\Delta(\partial\varphi'/\partial z)=(\partial/\partial z)(\varphi'_U+\varphi'_L) \quad \begin{matrix}\text{(a source strength}\\ \text{distribution)}\end{matrix} \tag{6}$$

For symmetric flow, such as in diaphragm and symmetric aerofoils, $\varphi'_U=\varphi'_L$, whereas for antisymmetric flow (i.e., camber and lift problems), $\varphi'_U=-\varphi'_L$. Using the doublet and source strength definitions of Eqs. (5) and (6), the integral relation for the velocity potential for a general interference problem is given by

$$2\pi\varphi'(X_0)=\sum_{el}\left[\iint\Delta\varphi'(X)\frac{\partial\psi}{\partial z}\,dxdy-\iint\psi\Delta\frac{\partial\varphi'}{\partial z}\,dxdy\right] \tag{7}$$

where Σ_{el} denotes summation over all elements in the domain of dependence, excluding diaphragms. Numerical handling of the second integral (the source superposition method), has been discussed elsewhere.[10,15] This study considers the development of the doublet superposition method for thin surfaces, defined by

$$2\pi\varphi'(X_0)=\iint\Delta\varphi'(X)(\partial\psi/\partial z)\,dxdy \tag{8}$$

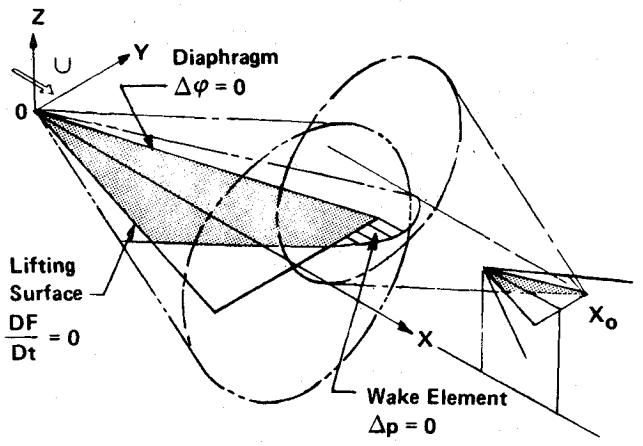

Fig. 1 General mixed dependence domain of downwash point X_0.

The domain of dependence now includes only the lifting surfaces themselves and the wake region, diaphragms being unnecessary.

In the transformed local coordinates, $(\partial/\partial z)(\ ) = -(\partial/\partial z_0)(\ )$. Hence, Eq. (8) may be written as

$$2\pi\varphi'(X_0) = -\iint \Delta\varphi'(X)\,(\partial\psi/\partial z_0)\,dxdy \tag{9}$$

The generalized Green's function ψ is related to two elementary solutions of Eq. (2), ψ_1 *and* ψ_2, which vanish on the aft Mach boundary, and, from Ref. 3,

$$\psi = (\partial\psi_1/\partial x_0) + k'^2\psi_2 = \cos k'R/R \tag{10}$$

where

$$R = [(x_0-x)^2 - (y_0-y)^2 - (z_0-z)^2]^{1/2}$$

is the hyperbolic radius.

From Leibnitz's theorem, Jones[3] has shown that, since $\Delta\varphi = 0$ on the leading edge and $\psi_1 = \psi_2 = 0$ on the aft Mach cone, Eq. (9) can be written as

$$2\pi\varphi'(X_0) = -(\partial/\partial z_0)\iint \Delta\varphi'(X)\,\psi\,dxdy \tag{11}$$

Now, using the transformation for φ' from Eq. (3), the integral relation for the velocity potential at X_0 is given by

$$2\pi\varphi(X_0) = -(\partial/\partial z_0)\iint \exp[-ik'M(x_0-x)]\,\Delta\varphi(X) \cdot (\cos k'R/R)\,dxdy \tag{12}$$

Finite Element Model

In the finite element method, the unknown doublet distribution $\Delta\varphi$ within an element can be represented by

$$\Delta\varphi(X) = \Omega(X)\Delta\phi \tag{13}$$

where $\Omega(X)$ is a transformation matrix function,[19] and $\Delta\phi$ is a vector of velocity potential jumps at the element nodes. A linear distribution of $\Delta\varphi(x)$ within a triangular element is represented by

$$\Omega(X) = [1, (x_0-x), (y_0-y)]\,T \tag{14}$$

in which

$$T = \begin{bmatrix} 1 & x_0-x_1 & y_0-y_1 \\ 1 & x_0-x_2 & y_0-y_2 \\ 1 & x_0-x_3 & y_0-y_3 \end{bmatrix}^{-1}$$

and

$$\Delta\phi = \begin{Bmatrix} \Delta\phi_1 \\ \Delta\phi_2 \\ \Delta\phi_3 \end{Bmatrix}$$

is a column vector of velocity potential jumps at the vertices of a triangle (element nodes).

Using Eq. (13) in Eq. (12), the velocity potential can be written as

$$2\pi\varphi(X_0) = \sum_{el} [I_1 I_2 I_3].T.\Delta\phi \tag{15}$$

where

$$I_1 = -(\partial/\partial z_0)\iint \exp[-ik'M(x_0-x)]\cos k'R/R\,dxdy \tag{16}$$

represents that part of φ arising from the constant part of the potential distribution within the element,

$$I_2 = -(\partial/\partial z_0)\iint \exp[-ik'M(x_0-x)]\,(x_0-x) \times (\cos k'R/R)\,dxdy \tag{17}$$

represents the part due to the potential linear in x, and

$$I_3 = -(\partial/\partial z_0)\iint \exp[-ik'M(x_0-x)]\,(y_0-y) \times (\cos k'R/R)\,dxdy \tag{18}$$

represents the part due to the potential linear in y.

In order to determine the unknown velocity potentials $\Delta\phi$, the kinematic boundary conditions at the control point X_0 on the lifting surface and other boundary conditions have to be satisfied. The kinematic boundary conditions are given by

$$W\Delta\phi = d\eta/dt \tag{19}$$

where W is a normal velocity influence coefficient matrix (see Appendix and Ref. 25), and η is the deformation normal to the surface at X_0. The rows of W correspond to control points in the lifting surface (excluding leading edges) at which the kinematic boundary conditions are satisfied. The columns of W correspond to influencing potential distribution. Other boundary conditions to be satisfied (see Fig. 1) are 1) the doublet strength $\Delta\varphi = 0$ on the leading edge and diaphragm, and 2) the pressure difference Δp in the wake is zero.

Since $\Delta\phi_{1LE}, \Delta\phi_{2LE} = 0$ on the leading edges of wings 1 and 2, rows and columns corresponding to nodes on the leading edges are eliminated from the W matrix. Then Eq. (19) can be solved for $\Delta\phi_1$ and $\Delta\phi_2$ to give

$$\left\{\begin{array}{c} \Delta\phi_1 \\ \hline \Delta\phi_2 \end{array}\right\} = \left[\begin{array}{c|c} \tilde{W}_{11} & \tilde{W}_{12} \\ \hline \tilde{W}_{21} & \tilde{W}_{22} \end{array}\right] \left\{\begin{array}{c} d\eta_1/dt \\ \hline d\eta_2/dt \end{array}\right\} \tag{20}$$

where

$$\left[\begin{array}{c|c} \tilde{W}_{11} & \tilde{W}_{12} \\ \hline \tilde{W}_{21} & \tilde{W}_{22} \end{array}\right] = \left[\begin{array}{c|c} W_{11} & W_{12} \\ \hline W_{21} & W_{22} \end{array}\right]^{-1} \tag{21}$$

and the subscripts denote the lifting surfaces 1 and 2. Having determined the velocity potential distribution on the lifting surfaces, the generalized aerodynamic coefficients $\tilde{Q}_{ij}$ can be determined.[15]

Computational Method

The determination of the velocity potential field on oscillating surfaces of an arbitrary configuration has been reduced to an integral relation [Eq. (20)] between the velocity potential doublet distribution $\Delta\phi$ and the normal induced velocity distribution on the lifting surfaces $d\eta/dt$. Boundary conditions such as $\Delta\phi = 0$ on the diaphragm and $\Delta p = 0$ in the wake field have been recognized in formulating the deterministic set of linear equations (20).

The integrals in Eq. (16, 17, and 20) leading to the evaluation of the velocity components require special consideration, since the generalized Green's function ψ behaves in a singular manner as the integration approaches the Mach boundary. Generally, Hadamard's finite part method is employed to evaluate such integrals. Alternatively, Jones[20] has suggested a closed-form integration method, briefly described in the Appendix. In order to obtain closed-form integrals, the Green's function $\psi = \cos k'R/R$ is expressed in a power series. Only those terms which are nonanalytic in the dependence domain are evaluated in closed form, whereas the analytic terms in the series are evaluated numerically. All of the area integrals have been transformed further to contour integrals.[25]

Since the $\cos k'R$ term is expressed by a simple power series, the convergence will depend on the magnitude of the

frequency parameter k'. In the dependence domain, close to Mach boundary, R is small. Hence, only a few terms beyond the first are necessary. For elements far from control point X_0 (R large), their contribution to velocity components is small, and once again only a few terms are necessary. Convergence of power series is, however, slow compared to Bessel series. In some examples, at $M=1.05$ and $k=1.0$, as many as 12 terms were required for less than 5% contributions from the additional terms. However, if generalized aerodynamic coefficients are required for a number of frequency parameters k, as is usually the case in practice, computational efficiency favors a power series expression, since the terms involving frequency, i.e., Cj and $e^{-ik'M\xi}$, are uncoupled from geometric parameters. This is not the case for a Bessel series (see Appendix).

Discretization of the lifting surface in the velocity potential method has some bearing on the modal distribution of doublets $\Delta\varphi$ within an element. For triangular elements with a linear distribution of $\Delta\varphi$, control points are chosen at the vertices in order to establish a deterministic set of equations for the potential. For an arbitrary grid system, contour integrals along a line 1-3 passing through a control point (Fig. 2a) result in a term $m^2/(1-m^2)^{1/2}$, where m is the slope of the line. If $m \approx \pm 1$, i.e., close to Mach boundary, an ill-conditioned system of equations results from this idealization. On the other hand, if elements based on characteristic parallelograms and their diagonals are considered, such as in Fig. 2b, the integrals of the self-induced elements may be evaluated in closed form. This results in a well-conditioned system of equations. Figure 3 shows a typical characteristic-based grid of a wing-control combination. For different Mach numbers, characteristic mesh can be generated automatically.

All edges are defined exactly, a distinct advantage over conventional Mach and characteristic box methods. In the wake field, since the potential doublet is related to the trailing edge values, the wake sheet can be approximated by rectangular strips bound by the trailing edge and Mach boundary (Fig. 1 and Ref. 25). The integration of the first two terms in the series is evaluated in closed form, whereas the remaining terms are computed numerically. Along the Mach hyperbola the first two terms are given merely by the terminal values of the contour, and the higher-order terms are zero.[25]

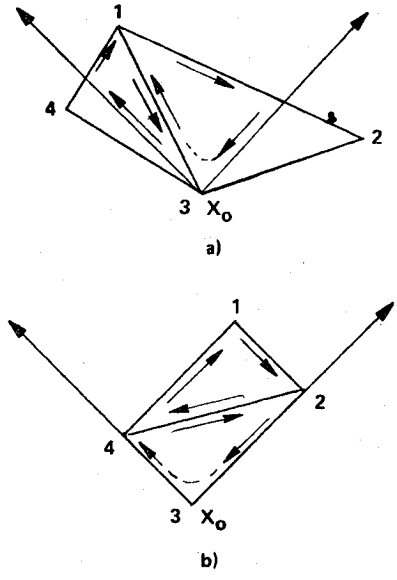

Fig. 2 Element configurations.

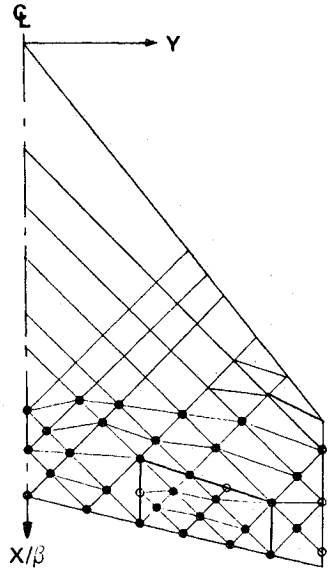

Fig. 3 Typical characteristic grid idealization with control surface. • Denotes downwash point at which the kinematic boundary conditions are satisfied. ○ Denotes ancillary grid point at which the velocity potential is interpolated but the downwash is not computed.

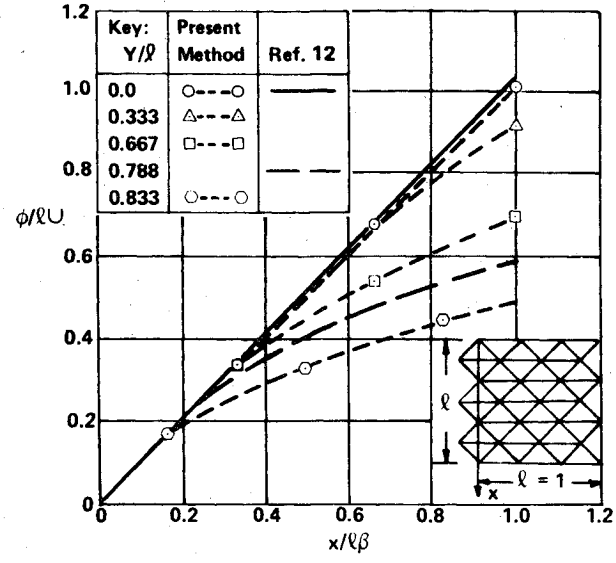

Fig. 4 Velocity potential $\phi(x,y,0^+)$ on a rectangular $A=2$ wing at unit incidence in a steady flow at $M=2^{1/2}$.

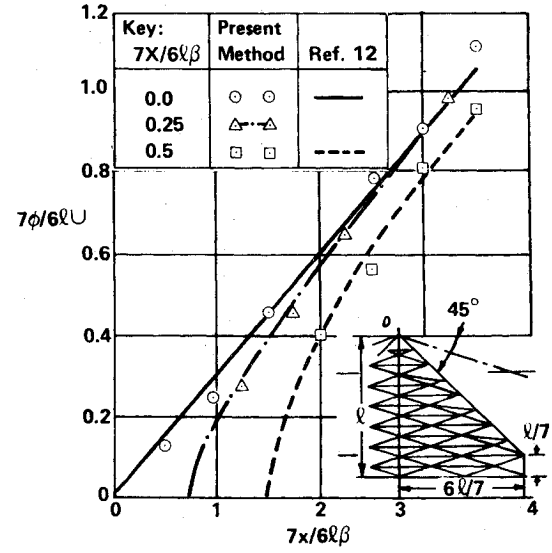

Fig. 5 Velocity potential $\phi(x,y,0^+)$ on a cropped delta wing at unit incidence in steady flow at $M=1.054$.

Results and Discussion

To assess the solution accuracy and the versatility of the finite element approach to the integrated velocity potential method, a limited number of calculations have been performed. Velocity potential distributions and generalized aerodynamic coefficients have been compared with available results. In all of the examples, the lifting surfaces have been represented by an assembly of triangular elements defined by arbitrarily spaced characteristic lines and the true surface edges. The center chord of the wing has been considered as the reference length l, unless redefined in the specific examples.

Isolated Wings

Figure 4 compares the perturbed velocity potential distribution on a rectangular wing in steady supersonic flow at

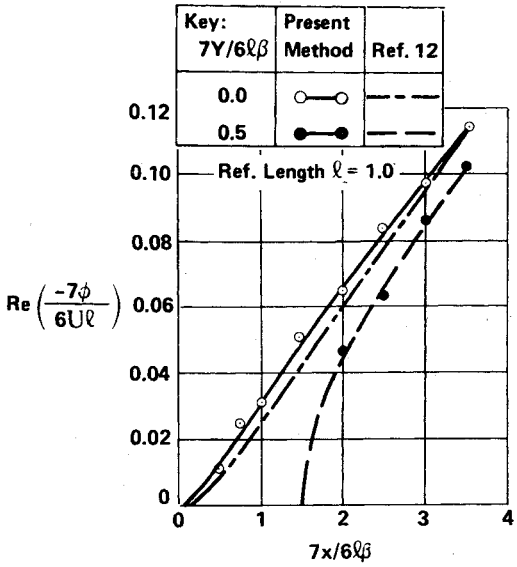

Fig. 6 Real part of the velocity potential (ϕ) on a cropped delta wing oscillating in translation with amplitude $\eta(x,y) = 2/7$ for frequency parameter $k = 0.4743$ at $M = 1.054$.

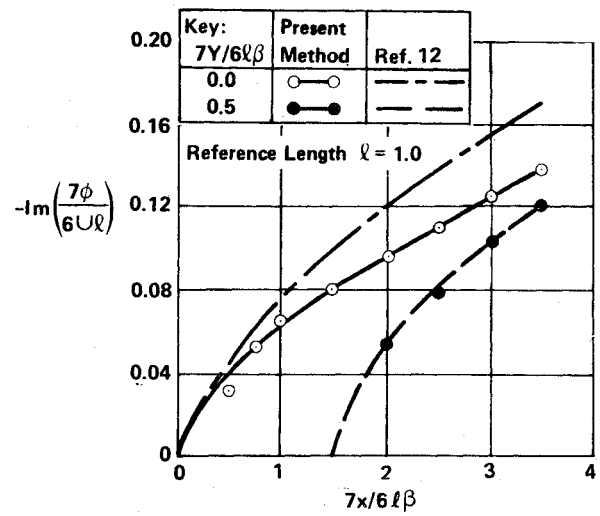

Fig. 7 Imaginary part of the velocity potential (θ) on a cropped delta wing oscillating in translation with amplitude $\eta(x,y) = 2/7$ for frequency parameter $k = 0.4743$ at $M = 1.054$.

Table 1 Comparison of generalized aerodynamic coefficients at Mach number 1.2 for mode; $\eta_1 = 1.0$, $\eta_2 = x - 0.5$ (reference length l = center line chord)

Config.	Method		Present	Woodcock (Ref 21)		Present	Woodcock (Ref 21)		Present	Woodcock (Ref 21)	
				M9*	M19**		M9*	M19**		M9*	M19**
Wing	Chord Nodes / Span Nodes		6/5	34/30	30/20	6/5	34/30	30/20	6/5	34/30	30/20
AGARD Rectangular Wing AR = 2.0	Frequency Parameter.K		0.0	0.0	0.0	0.3	0.3	0.3	0.6	0.6	0.6
	Re	(Q_{11})	0.0	0.0	0.0	0.220	0.205	0.189	0.414	0.749	0.348
	Re	(Q_{12})	3.800	3.951	3.750	3.340	3.531	3.37	2.780	3.058	2.840
	Re	(Q_{21})	0.0	0.0	0.0	-0.008	-0.005	-0.005	-0.114	-0.026	-0.107
	Re	(Q_{22})	-0.310	-0.398	-0.368	-0.350	-0.446	-0.411	-0.280	-0.427	-0.380
	Im	(Q_{11})				0.980	1.060	1.000	1.560	1.820	1.620
	Im	(Q_{12})				-0.590	-0.545	-0.500	-0.386	-0.940	-0.288
	Im	(Q_{21})				-0.112	-0.141	-0.130	-0.228	-0.310	-0.285
	Im	(Q_{22})				-0.159	-0.177	-0.165	0.414	0.350	0.450
AGARD Tapered Wing AR = 1.45	Frequency Parameter.K		0.0	0.0	0.0001	0.5	0.5	0.5	1.0	1.0	1.0
	Re	(Q_{11})	0.0	0.0	0.0	0.015	0.011	-0.023	-0.264	-0.369	-0.404
	Re	(Q_{12})	3.8	4.140	3.930	3.780	3.811	3.671	4.05	4.190	4.070
	Re	(Q_{21})	0.0	0.0	0.0	-0.310	-0.278	-0.283	-0.675	-0.722	-0.708
	Re	(Q_{22})	0.082	0.059	-0.012	0.485	0.287	0.244	0.965	0.858	0.802
	Im	(Q_{11})				1.680	1.720	1.650	3.360	3.650	3.550
	Im	(Q_{12})				1.010	0.840	0.860	1.870	1.600	1.580
	Im	(Q_{21})				0.141	0.020	0.004	0.645	0.546	0.502
	Im	$(Q_{22}$				1.320	1.250	1.230	1.83	1.790	1.740

* Ref 22
** Ref 12

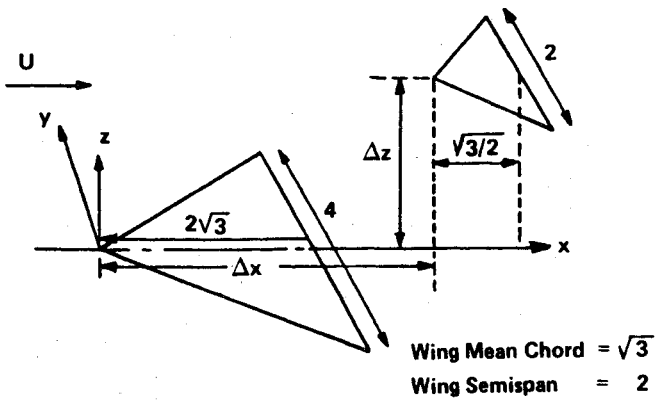

Fig. 8 Interacting configuration of triangular wing-tail combination.

$M=2^{1/2}$ and unit incidence. The results from four grids on the chord compare well with those from 16 characteristic boxes used in Ref. 12. Similarly, Fig. 5 compares the velocity potential distribution on a cropped delta wing in steady flow at $M=1.054$ and constant incidence. By increasing the number of chord elements, the waviness in the potential distribution can be minimized. Once again, the velocity potential distribution from eight grids on the center chord compares well with that from 16 characteristic boxes in Ref. 12.

The real and imaginary parts of the velocity potential distribution on a cropped delta wing in heave motion at a reduced frequency $k=0.4743$ and $M=1.054$ are shown in Figs. 6 and 7. The real part agrees very well with Ref. 12, whereas the imaginary part differs significantly for the centerline chord.

The generalized aerodynamic coefficients for two AGARD planforms are compared in Table 1 with two source superposition methods M9 and M19,[22,12] as reported by Woodcock.[21] In the present analysis, six center chord nodes and five spanwise nodes were used, whereas in Ref. 21, approximately 30 and 20 boxes were used in the chord and span directions, respectively. The generalized aerodynamic coefficients Q_{ij} for the rectangular wing and the tapered wing are in very good agreement with the results reported in Ref. 21.

Interacting Wings

The delta wing-tail combination[17] is shown in Fig. 8. The apex of the tail was placed vertically above the wing trailing edge, and the vertical separation was varied. In order to present the results in a form reported by Refs. 17 and 23, the generalized aerodynamic coefficients are defined as $Q_{ij}=\rho U^2 l^2 s(Q'_{ij}+kQ''_{ij})$, where reference lengths are $l=3^{1/2}$ semichord, and $s=2$, the semispan. The damping coefficients Q''_{ij} in heave and pitch motion are compared in Table 2 with Refs. 17, 23, and 15 for three vertical separations: $z/l=2.6$, 0.52, and 0.26. For $z/l=2.6$, wing and tail do not interact; for $z/l=0.52$, the tail domain of dependence includes the wing

	x	y	z
a	0	0	0
b	2.25	0	0
c	2.75	1.00	0
d	3.70	1.00	0
e	2.70	0	0
f	4.00	0	0
g	3.90	1.00	0
h	4.25	1.00	0
e′	3.10	0	0.60
f′	4.40	0	0.60
g′	4.30	1.00	0.60
h′	4.65	1.00	0.60
e″	3.55	0	1.20
f″	4.85	0	1.20
g″	4.75	1.00	1.20
h″	5.10	1.00	1.20
e‴	2.70	0	0
f‴	4.00	0	0
g‴	3.90	1.00	0.50
h‴	4.25	1.00	0.50
i	2.50	0	0
j	4.20	0	0
k	3.70	0	1.20
ℓ	4.60	0	1.20

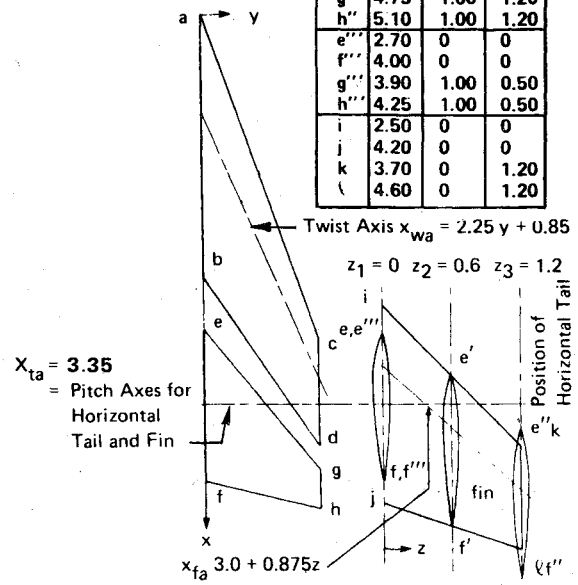

Fig. 9 AGARD wing-horizontal, tail-vertical fin combination.

Table 2 Comparison of the damping coefficient Q''_{ij} delta wing-tail configuration at $M=1.44$, $K=0.01$ modes: $\eta_1=x-\frac{2}{3}$

Lifting surfaces		Wing contribution		Tail contribution		Wing + Tail			
		Present method, 46 elements	Ref. 17, ... 300 elements	Present method, 21 elements	Ref. 17, ... 50 elements	Present method, 67 elements	Ref. 17, ... 350 elements	Ref. 23 ...	Ref. 15, ... 65 elements
$\Delta z/l=2.6$	Q''_{11}[a]	2.720	2.806	0.460	0.477	3.180	3.282	...	...
	Q''_{12}	0.062	0.173	0.400	0.385	0.462	0.214	...	...
	Q''_{21}	0.124	0.016	0.473	0.483	0.597	0.499	...	...
	Q''_{22}	0.588	0.579	0.396	0.395	0.984	0.974	...	...
$\Delta z/l=0.52$	Q''_{11}	2.720	...	0.450	...	3.170	3.028	2.664	...
	Q''_{12}	0.062	...	0.001	...	0.061	0.141	0.111	...
	Q''_{21}	0.124	...	0.460	...	0.584	0.240	0.188	...
	Q''_{22}	0.588	...	0.033	...	0.621	0.896	0.601	...
$\Delta z/l=0.26$	Q''_{11}	2.720	...	0.322	...	3.042	2.954	2.680	2.647
	Q''_{12}	0.062	...	0.193	...	0.255	0.170	0.096	0.667
	Q''_{21}	0.124	...	0.322	...	0.440	0.171	0.209	0.428
	Q''_{22}	0.588	...	0.210	...	0.798	0.934	0.598	1.174

[a] Generalized aerodynamic coefficient is defined here as $Q_{in}=\rho U^2 l^2 s(Q'_{ij}+kQ''_{ij})$, where $l=3^{1/2}$ and $s=2.0$.

Table 3 Antisymmetric modes

Wing	Tail	
$q_1 = y(x-2.75\|y\|-0.85)$	0,	twist
$q_2 = y\|y\|$	0,	bending
$q_3 = 0$	y,	roll
$q_4 = 0$	sign(y) $(x-3.35)$,	pitching

surface; for $z/l = 0.26$, the tail domain of dependence includes wing surface and wake; and for $z/l = 2.6$, the direct dampings from wing, tail, and wing plus tail are in good agreement with Ref. 17 to within 3%. The cross-damping terms from the tail are also within 3%, but the wing contributions (though of less significance) do not agree well.

For $z/l = 0.26$, the trend of the heave-induced terms continues, but there is some recovery in the pitch-induced tail contributions. The total results for the direct dampings com-

Table 4 Comparison of generalized aerodynamic coefficients Q_{ij} for AGARD wing-tail interference at $M = 3.0$ and $\Delta Z/L = 0.0$

			$k=0$		$k=1.5$		
Generalized force in	Caused by pressure in	i,j	$Re(Q_{ij})$	$Im(Q_{ij})$	$Re(Q_{ij})$	$Im(Q_{ij})$	Methods
Wing twist	Wing twist	1,1	0.0226	0.0	0.0966	0.1486	Ref. 22
			0.0208	0.0	0.1002	0.1463	Ref. 24
			0.0387	0.0	0.1059	0.1446	Present
Wing bending	Wing twist	2,1	0.3035	0.0	0.3846	0.0890	Ref. 22
			0.3020	0.0	0.3740	0.0890	Ref. 24
			0.2662	0.0	0.2710	0.1207	Present
Tail roll	Wing twist	3,1	0.2152	0.0	0.0394	0.0769	Ref. 22
			0.2137	0.0	0.0463	0.0696	Ref. 24
			0.2660	0.0	0.1200	0.0351	Present
Wing twist	Wing bending	1,2	...	...	−0.0700	0.0309	Ref. 22
			...	...	−0.0720	0.0327	Ref. 24
			...	...	−0.0294	0.0801	Present
Wing bending	Wing bending	2,2	...	...	0.0730	0.2335	Ref. 24
			...	...	0.0167	0.2464	Present
Tail roll	Wing bending	3,2	...	...	0.1477	0.0160	Ref. 24
			...	...	0.1146	0.0611	Present
Tail pitch	Wing bending	4,2	...	...	0.1033	0.0197	Ref. 22
			...	...	0.0988	0.0167	Ref. 24
			...	...	0.093	−0.0857	Present
Tail roll	Tail roll	3,3	...	...	0.0168	0.2560	Ref. 22
			...	...	0.0700	0.3171	Present
Tail pitch	Tail roll	4,3	...	...	0.005	0.1786	Ref. 22
			...	...	0.0365	0.228	Present
Tail roll	Tail pitch	3,4	0.4665	0	0.4517	0.1632	Ref. 22
			0.4688	...	0.4410	0.2168	Present
Tail pitch	Tail pitch	4,4	o.2882	0	0.2965	0.2588	Ref. 22
			0.2873	...	0.3162	0.3010	Present

Table 5 Comparison of generalized aerodynamic coefficients Q_{ij} for AGARD wing-tail interference at $M = 3.0$ and $\Delta Z/L = 0.6$

			$K=0.0$		$k=1.5$		Methods
Generalized force in	Caused by pressure in	i,j	$Re(Q_{ij})$	$Im(Q_{ij})$	$Re(Q_{ij})$	$Im(Q_{ij})$	
Wing twist	Wing twist	1,1	0.0340	...	0.0913	0.1462	Ref. 23
			0.0387	...	0.1059	0.1446	Present
Wing bending	Wing twist	2,1	0.3160	...	0.3801	0.0890	Ref. 23
			0.2661	...	0.2710	0.1207	Present
Tail roll	Wing twist	3,1	0.0732	...	0.0132	0.1024	Present
Tail pitch	Wing twist	4,1	0.0957	...	0.0856	0.0541	Ref. 23
			0.0412	...	0.0068	0.0817	Present
Wing twist	Wing bending	1,2	...	...	−0.0746	0.0301	Ref. 23
			...	...	−0.0294	0.0801	Present
Wing bending	Wing bending	2,2	...	...	−0.0729	0.2447	Ref. 23
			...	...	0.0167	0.2464	Present
Tail roll	Wing bending	3,2	...	...	−0.0491	0.0615	Ref. 23
			...	...	−0.0715	0.0012	Present
Tail pitch	Wing bending	4,2	...	...	−0.0406	0.0485	Ref. 23
			...	...	−0.0602	0.0104	Present
Tail roll	Tail roll	3,3	...	...	0.0163	0.2622	Ref. 23
			...	...	0.0700	0.3170	Present
Tail pitch	Tail roll	4,3	...	...	0.0072	0.1864	Ref. 23
			...	...	0.0365	0.2208	Present
Tail roll	Tail pitch	3,4	0.4683	...	0.4539	0.1749	Ref. 23
			0.4688	...	0.4408	0.2159	Present
Tail pitch	Tail pitch	4,4	0.2944	...	0.3074	0.2219	Ref. 23
			0.2873	...	0.3161	0.3010	Present

pare well with Refs. 15, 17, and 23. The cross-dampings are generally within the scatter of these same references.

As an additional example in the interfering case, the generalized aerodynamic coefficients were calculated for the AGARD wing-tail configuration shown in Fig. 9. Four antisymmetric modes of the form given in Table 3 were considered, in order to obtain isolated and interfering components of Q_{ij} contributing to the total aerodynamic forces. At Mach number $M=3.0$, the wing and tail surfaces were represented by 66 and 47 triangular elements, respectively, whereas in Ref. 23, 510 boxes on wing and 264 on tail were used. The computed results were compared with those in Ref. 23 and 24.

The coplanar results for the reduced frequencies $k=(\omega l/U)=0$ and 1.5 are compared with Ref. 23 and 24 in Table 4. Note that the reference length $l=1.0$, the semispan of the wing. The generalized coefficients Q_{ij} for $\Delta z/l=0.6$ are compared with Ref. 23 in Table 5. In spite of large differences in the number of elements used, the noninterfering terms of Q_{ij} for tail modes are in very good agreement with Refs. 23 and 24 but do not compare so well for elastic modes of the wing. The interfering components of Q_{ij}, i.e., forces in tail mode due to wing modes, have the following general trends: the trehds of Refs. 23 and 24 agree in magnitude but not in sign, and the results of Ref. 23 and the present method agree in sign but differ in magnitude. It appears that the number of elements used on wing surface is not enough to represent elastic deformation. However, for rigid body modes, the convergence is seen to be rapid.

Conclusions

The integrated velocity potential method for the determination of unsteady supersonic aerodynamic forces on interacting lifting surfaces has been developed. Normal and sidewash integrals have been derived, including closed-form singular integrals. Interacting lifting surfaces may be discretized by an assembly of characteristic based triangles which match exactly all surface edges. Wakes are represented by rectangular strip elements. A number of examples have been presented, and the results have compared well with the existing results.

Appendix

This section briefly describes the method of evaluating singular functions without the use of Hadamard's finite part integral technique. The generalized Green's function is expressed in a power series, i.e.,

$$\psi=\cos k'R/R=\Sigma C_j R^{2j-1};j=0,1,2\ldots \tag{A1}$$

where

$$C_j=(-k'^2)^j/2j! \tag{A2}$$

In the transformed coordinates, the element is assumed to lie in the plane $z=0$. Let

$$\xi=x_0-x,\eta=y_0-y \tag{A3}$$

Then the integrals I_1, I_2, and I_3 from Eqs. (16-18) are rewritten as

$$I_1=\Sigma C_j[-(\partial/\partial z_0)\iint e^{-ik'M\xi}R^{2j-1}(\xi,\eta)\,d\eta];j=0,1,2\ldots \tag{A4}$$

$$I_2=\Sigma C_j[-(\partial/\partial z_0)\iint e^{-ik'M\xi}\xi R^{2j-1}(\xi,\eta)\,d\xi d\eta];j=0,1,2\ldots \tag{A5}$$

$$I_3=\Sigma C_j[-(\partial/\partial z_0)\iint e^{-ik'M\xi}\eta R^{2j-1}(\xi,\eta)\,d\xi d\eta];j=0,1,2\ldots \tag{A6}$$

The velocity components w and v can be evaluated by differentiating the integrals I_1, I_2, and I_3 with respect to z_0 and y_0, respectively. Evaluation of these integrals for normalwash and sidewash components is described below for each term in the series.

Differentiating Eq. (15) with respect to z_0, the normal velocity component is given by

$$2\pi w=2\pi\frac{\partial\varphi}{\partial z_0}=\left[\frac{\partial I_1}{\partial z_0}\frac{\partial I_2}{\partial z_0}\frac{\partial I_3}{\partial z_0}\right]T\Delta\phi$$

Evaluation of typical, singular integrals is as follows. For integral I_1 for $j=0$, i.e., I_1^0,

$$I_1^0=-(\partial/\partial z_0)\oint e^{-ik'M\xi}\int[d\eta/(r^2-\eta^2)^{1/2}]\,d\xi \tag{A7}$$

where $r^2=\xi^2-z_0^2$. Integrating with respect to η

$$I_1^0=-(\partial/\partial z_0)\oint e^{-ik'M\xi}\sin^{-1}(\eta/r)\,d\xi \tag{A8}$$

where $\oint$ denotes contour integration along the element boundaries, taken in a clockwise sense.

Case A: On the Mach Boundary

If the contour integration is along the Mach boundary (hyperbola), $\eta/r=\pm 1$, and hence $\sin^{-1}(\eta/r)=\text{sign}(\eta)\,\pi/2\equiv(\pi/2)(\eta)$. Then the velocity component is given by

$$w_1^0=\partial I_1{}^0/\partial z_0=ik'M(\pi/2)(\eta)\left[(\partial\xi/\partial z_0)^2 e^{-ik'M\xi}\right]_{\xi_L}^{\xi_u} \tag{A9}$$

where

$$\partial\xi/\partial z_0=1 \quad \text{if} z_0=0 \text{ and } \eta=0$$

$$=z_0/(\eta^2+z_0^2)^{1/2} \text{ otherwise}$$

Case B: Off the Mach Boundary

Differentiating Eq. (A8) with respect to z_0,

$$I_1^0=-z_0\oint[e^{-ik'M\xi}\eta/r^2R(\xi)]\,d\xi \tag{A10}$$

Let $\eta=m\xi+\alpha$ be an equation to the line, where m is its slope and α a constant.

The presence of the exponential term in Eq. (A10) complicates the evaluation of the singular integral. However, if the interval of the contour integral is divided into a number of subintervals and the exponential term within each interval is assumed constant, Eq. (A10) integrates to give

$$I_1^0=-\sum_{\xi_L}^{\xi_u}\exp[-ik'M\xi_{\text{av}}][G(\xi)]_{\xi_i}^{\xi_i+1} \tag{A11}$$

where $G(\xi)=\frac{1}{2}(\tan^{-1}A-\tan^{-1}A')$, in which

$$A(\xi)=N(\xi)/R(\xi) \tag{A12a}$$

$$A'(\xi)=N'(\xi)/R(\xi) \tag{A12b}$$

$$N(\xi)=-\eta+[z_0/(\alpha+mz_0)](\xi-z_0) \tag{A12c}$$

$$N'(\xi)=-\{\eta+[z_0/(\alpha-mz_0)](\xi+z_0)\} \tag{A12d}$$

$$\xi_{\text{av}}=\frac{(\xi_i+\xi_{i+1})}{2} \tag{A12e}$$

The normal-wash component is given by

$$w_1^0=\partial I_1^0/\partial z_0=-\sum_{\xi_L}^{\xi_u}\exp[-ik'M\xi_{\text{av}}][\partial G/\partial z_0]_{\xi_i}^{\xi_i+1} \tag{A13}$$

where

$$\frac{\partial G}{\partial z_0} = \frac{1}{2}\left(\frac{A^*}{1+z_0{}^2 A^{*2}}\right) \tag{A14a}$$

$$A^* = \frac{2R(\alpha\xi + mz_0{}^2)}{(\alpha^2 - m^2 z_0{}^2)(R^2+\eta^2) - z_0{}^2(R^2-\eta^2)} \tag{A14b}$$

In the planar case, as $z_0 \to 0$

$$w_1^0 = -\sum_{\xi_L}^{\xi_u} \exp[-ik'M\xi_{av}]\,[R(\xi)/\alpha\xi]_{\xi_i}^{\xi_i+1}, \alpha \neq 0 \tag{A15}$$

If $\alpha = 0$, i.e., the line passes through the field point X_0 (Fig. 2a),

$$w_1^0 = [m/(1-m^2)^{1/2}] \sum_{\xi_L}^{\xi_u} e^{-ik'M\xi} \left[\frac{1}{\xi}\right]_{\xi_i}^{\xi_i+1} \quad \text{if } \xi \neq 0 \tag{A16}$$

$$= 0 \text{ if } \xi = 0$$

Similarly, all singular integrals leading to the velocity components can be evaluated in closed form (see, for example, Ref. 25).

References

[1] Garrick, I. E. and Rubinow, S. I., "Theoretical Study of Air Forces on An Oscillating or Steady Thin Wing in a Supersonic Main Stream," NACA Rept. 827, 1947.

[2] Ashley, H., "Supersonic Airloads on Interfering Lifting Surfaces by Aerodynamic Influence Coefficient Theory," The Boeing Co., Seattle, Wash., Rept. D2-22067, Nov. 1962.

[3] Jones, W. P., "Supersonic Theory for Oscillating Wings of Any Planform," Aeronautical Research Council, R&M 2655, June 1948.

[4] Watkins, C. E. and Berman, J. H., "On the Kernel Function of the Integral Equation Relating Lift and Downwash Distributions of Oscillating Wings in Supersonic Flow," NACA Rept. 1257, 1956.

[5] Harder, R. L. and Rodden, W. P., "Kernel Function for Non-Planar Oscillating Surfaces in Supersonic Flow," *Journal of Aircraft*, Vol. 8, Aug. 1971, pp. 667-679.

[6] Heaslet, M. A., Lomax, H., and Jones, A. L., "Volterra's Solution of the Wave Equation as Applied to Three-Dimensional Supersonic Airfoil Problems," NACA Rept. 889, 1947.

[7] Richardson, J. R., "A Method for Calculating the Lifting Forces on Wings (Unsteady Subsonic and Supersonic Lifting-Surface Theory)," British Aeronautical Research Council, R&M 3157, 1955.

[8] Cunningham, H. J., "Improved Numerical Procedure for Harmonically Deforming Lifting Surfaces from the Supersonic Kernel Function Method," *AIAA Journal*, Vol. 4, Nov. 1966, pp. 1961-1968.

[9] Cunningham, A. M., Jr., "A Kernel Function Method for Computing Steady and Oscillatory Supersonic Aerodynamics with Interference," *Journal of Aircraft*, Vol. 11, Oct. 1974, pp. 609-615.

[10] Ii, J. M., Boreland, C. J., and Hogley, J. R., "Prediction of Unsteady Aerodynamic Loadings of Non-Planar Wings and Wing-Tail Configurations in Supersonic Flow. Part I – Theoretical Development, Program Usage, and Application," Air Force Flight Dynamics Lab., Wright-Patterson AFB, Ohio, AFFDL-TR-71-108, March 1972.

[11] Kramer, G. D. and Kaylon, G. E., "Prediction of Unsteady Aerodynamic Loadings of Non-Planar Wings and Wing-Tail Configurations in Supersonic Flow. Part II," Air Force Flight Dynamics Lab., Wright-Patterson AFB, Ohio, AFFDL-TR-71-108, March 1972.

[12] Stark, V. J. E., "Calculation of Aerodynamic Forces on Two Oscillating Finite Wings at Low Supersonic Mach Numbers," SAAB TN 53, 1964.

[13] Appa, K., "Kinematically Consistent Unsteady Aerodynamic Coefficients in Supersonic Flow," *International Journal for Numerical Methods in Engineering*, Vol. 2, Oct. 1970, pp. 495-507; (also National Aeronautical Laboratories, India, TN-9, March 1968.)

[14] Appa, K. and Smith, G. C. C., "Further Developments in Consistent Unsteady Supersonic Aerodynamic Coefficients," *Journal of Aircraft*, Vol. 9, Feb. 1972, pp. 157-167.

[15] Appa, K. and Smith, G. C. C., "Development and Applications of Supersonic Unsteady Consistent Aerodynamics for Interfering Parallel Wings," NASA CR-2168, March 1973.

[16] Allen, D. J. and Sadler, D. S., "Oscillatory Aerodynamic Forces in Linearized Supersonic Flow for Arbitrary Frequencies, Planforms and Mach Numbers," British Aeronautical Research Council, R&M 3415, 1963.

[17] Woodcock, D. L. and York, E. J., "A Supersonic Box Collocation Method for the Calculation of Unsteady Airforces of Tandem Surfaces," *Proceedings of AGARD Symposium on Unsteady Aerodynamics for Aeroelastic Analyses of Interfering Surfaces*, AGARD-CP-80-71, 1971.

[18] Chen, L. T., Suciu, E. O., and Morino, L., "A Finite Element Method for Potential Aerodynamics Around Complex Configurations," *AIAA Journal*, Vol. 13, March 1975, pp. 368-374.

[19] Appa, K. and Smith, G. C. C., "Finite Element Approach to the Integrated Potential Formulation of General Unsteady Supersonic Aerodynamics," NASA-CR-112296, 1973.

[20] Jones, W. P., private communication to K. Appa, Dec. 1973.

[21] Woodcock, D. L. (ed.), "A Comparison of Methods Used in Lifting Surface Theory," *Supplement to the Manual on Aeroelasticity*, Pt. VI, NATO-AGARD Rept. 583, 1971.

[22] Fenain, M. and Guiraud-Valle, D., "Numerical Calculations of Wings in Steady or Unsteady Supersonic Flow. Part 1: Steady Flow, Part 2: Unsteady Flow," *La Recherche Aerospatiale*, No. 115, 1966-1967.

[23] Pollock, S. J. and Huttsell, L. J., "Applications of Three Unsteady Aerodynamic Load Prediction Methods," Air Force Flight Dynamics Lab., Wright-Patterson AFB, Ohio, 73-147, May 1974.

[24] Schmid, H. and Becker, J., "Contribution to the AGARD Program on Unsteady Aerodynamics for Interfering Lifting Surfaces," MBB Paper, 1973 (communicated by W. P. Rodden).

[25] Appa, K., "Integrated Potential Formulation of Unsteady Supersonic Aerodynamics for Interacting Wings," NASA CR-132547, Oct. 1974.